

# CD<sup>2</sup>: Fine-grained 3D Mesh Reconstruction with Twice Chamfer Distance

RONGFEI ZENG\*, MAI SU\*, and XINGWEI WANG, Northeastern University, China

Monocular 3D reconstruction is to reconstruct the shape of object and its other detailed information from a single RGB image. In 3D reconstruction, polygon mesh is the most prevalent expression form obtained from deep learning models, with detailed surface information and low computational cost. However, some state-of-the-art works fail to generate well-structured meshes, these meshes have two severe problems which we call Vertices Clustering and Illegal Twist. By delving into the mesh deformation procedure, we pinpoint the inadequate usage of Chamfer Distance(CD) metric in deep learning model. In this paper, we initially demonstrate the problems resulting from CD with visual examples and quantitative analyses. To solve these problems, we propose a fine-grained reconstruction method CD<sup>2</sup> with Chamfer distance adopted twice to perform a plausible and adaptive deformation. Extensive experiments on two 3D datasets and the comparison of our newly proposed mesh quality metrics demonstrate that our CD<sup>2</sup> outperforms others by generating better-structured meshes.

CCS Concepts: • **Computing methodologies** → **Reconstruction**; Shape representations.

Additional Key Words and Phrases: 3D reconstruction, machine learning, chamfer distance, mesh deformation

## ACM Reference Format:

Rongfei Zeng, Mai Su, and Xingwei Wang. 0. CD<sup>2</sup>: Fine-grained 3D Mesh Reconstruction with Twice Chamfer Distance. *J. ACM* 0, 0, Article 0 (0), 19 pages. <https://doi.org/XXXXXXX.XXXXXXX>

## 1 INTRODUCTION

Monocular 3D mesh reconstruction, boosted by deep learning, is a fundamental and fascinating technique in the community of computer vision. It aims to generate detailed 3D information of the object's surface, orientation, etc. in mesh format from a single 2D image [19]. The prevalent data format of mesh, which consists of hundreds of vertexes and faces, has plenty of features and advantages. For instance, mesh can efficiently and accurately capture the details of 3D objects' surfaces and describe almost every shape in the world, such as cars, boats, and airplanes in ShapeNet dataset [6]. Meanwhile, the quality of mesh has been drastically improved by the promising technique of deep learning and large-scale datasets in recent years [6, 31]. All these benefits empower 3D mesh reconstruction with deep learning to have widespread applications in 3D printing, automatic drive, virtual/augmented reality, medical diagnosis, and online shopping [20].

In the deep-learning-enabled mesh reconstruction, Chamfer Distance (CD) [2] is a universally-adopted and paramount component which is used as the loss function of deep learning model as well as the metric to measure quality of generated 3D mesh model. CD calculates the average of

\*Both authors contributed equally to this research.

Authors' address: Rongfei Zeng, [zengrf@swc.neu.edu.cn](mailto:zengrf@swc.neu.edu.cn); Mai Su, [sumai1998@foxmail.com](mailto:sumai1998@foxmail.com); Xingwei Wang, [wangxw@mail.neu.edu.cn](mailto:wangxw@mail.neu.edu.cn), Northeastern University, No.11 HEPING Region WENHUA Street, Shenyang, Liaoning, China, 110819.

Permission to make digital or hard copies of all or part of this work for personal or classroom use is granted without fee provided that copies are not made or distributed for profit or commercial advantage and that copies bear this notice and the full citation on the first page. Copyrights for components of this work owned by others than ACM must be honored. Abstracting with credit is permitted. To copy otherwise, or republish, to post on servers or to redistribute to lists, requires prior specific permission and/or a fee. Request permissions from [permissions@acm.org](mailto:permissions@acm.org).

© 0 Association for Computing Machinery.

0004-5411/0/0-ART0 \$15.00

<https://doi.org/XXXXXXX.XXXXXXX>

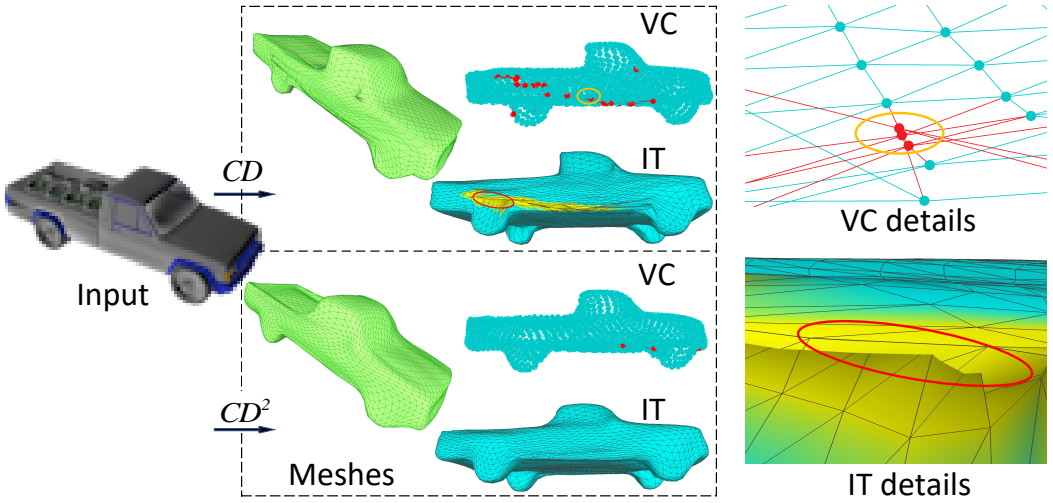


Fig. 1. IT and VC problems in 3D mesh reconstructions and our improvement with  $CD^2$ .

pair-wise nearest neighbour distance between the synthetic mesh and the ground-truth object. It is preferable due to its efficient computation and flexible applicability with different point numbers. The vast majority of impressive works such as Atlasnet [12], TMN [24] and Pixel2Mesh [37] employ CD as loss function or part of loss function for model training and achieve acceptable and impressive model performance.

However, CD has some intrinsic deficiencies and some previous studies have been published to identify them. For instance, Li shows that CD may suffer from the local optimum problem in its nearest neighbor search [14]. Wu reiterates that CD is insensitive to point density distribution and is prone to be impacted by outliers [39]. Jin demonstrates that CD may not be faithful visually and structurally [13]. Achlioptas finds that CD is inclined to generate overcrowded points in some visible areas of object in the input image [1]. Wagner empirically proves that directly optimizing CD will ignore details of some structure [34]. Meanwhile, researchers also propose some variant CD, such as structured CD [14], a sharper version of CD [16], adaptive CD [35], probabilistic CD [15], augmented CD [7], density-aware CD [39], etc., attempt to fix the defects of CD mentioned above.

Even worse, we find that CD still suffers from Illogical Twist (IT) and Vertex Clustering (VC) problems, which have not been declared in previous studies. As shown in Fig. 1, IT problem refers to the situation where some faces locally and irrationally intersect with others or interpose into some inner regions, while VC problem describes the scenario where many vertices of mesh cluster around a single ground-truth point. Empirically, both IT and VC problems are attributed to CD loss function which offers incorrect deformation direction in the brute-force nearest neighbour search. The consequence of these two problems is the performance degradation of mesh by wasting limited vertices in some invisible and overcrowded regions and distorting the mesh into an unusable structure. Furthermore, these severe problems might malfunction the downstream applications of 3D reconstruction, such as 3D printing, rendering, etc. In sum, IT and VC problems caused by CD should be considered seriously in mesh reconstruction.

In this paper, we deep dive into the IT and VC problems and endeavor to improve the quality of reconstructed mesh with the key idea of twice CD calculation in deep learning approach. In detail,

we start with the identification of IT and VC problems in both empirical and quantitative ways and then find that some vertices of generated mesh move in incorrect directions or at much aggressive speed. Following these observations, we provide our proposal CD<sup>2</sup> to perform a reasonable and fine-grained mesh generation process. The proposed CD<sup>2</sup> calculates the CD metric twice and excludes some excessively-moving vertices from further deformation with three criteria, which makes all the vertices deform with a comparable speed in a correct direction. Comparing with some impressive works on two datasets ShapeNet and Pix3D in several metrics, we demonstrate our scheme CD<sup>2</sup> can effectively and efficiently mitigate IT and VC problems and yield a fine-grained 3D mesh model.

The contributions of this paper are threefold:

- To the best of our knowledge, we are the first to identify IT and VC problems caused by CD in deep learning 3D reconstruction model and provide both visual examples and quantitative analyses of these problems.
- We propose an innovative approach CD<sup>2</sup> with twice CD calculation to mitigate IT and VC problems by moving vertices in a moderate speed and rational direction.
- Our CD<sup>2</sup> generates more plausible and fine-grained meshes than others, we also present several mesh quality metrics with faithful and appropriate measuring capability.

## 2 RELATED WORK

In this section, we review different methods of machine learning based 3D reconstruction and various representation forms, we then discuss the main metrics employed in these works, we summarize the existing problems concerned with Chamfer Distance revealed by recent works and some attempts to relieve these problems.

### 2.1 3D Reconstruction with Machine Learning

There exists a variety of studies in the field of 3D reconstruction from RGB images using promising machine learning models. In these studies, the output format to represent 3D objects includes point cloud [17, 23, 39], voxel [28, 36, 40], primitives[12], mesh[21], etc. Among them, mesh is more adaptable to complicated topology and can describe any 3D object accurately and efficiently. Some studies generate mesh objects using the form of signed distance fields [9] and implicit surfaces [22], while other impressive studies reconstruct mesh objects from a template with deformation methods, which are the concerns of this paper. For the deformation-based 3D mesh reconstruction, Kanazawa [32] proposed a novel framework which can produce 3D shape of a category-specific mesh by transforming a learned mean shape. Pontes [26] obtained a compact mesh representation with deformation method from a cube shape at first. Gkioxari [11] converted the coarse voxel to mesh by refining the vertices and edges with graph convolution network. Wang [37] progressively deformed an ellipsoid to the target object by utilizing the perceptual features from the images. Groueix [12] even supported mesh deformation from different amounts of spheres or squares because each batch represents one part of the target shape. Huang[42] combined multi-view renderings and a 3D human template to a deformation model and achieve photo-consistency human meshes. Chen [7] folded a 2D lattice to the implicit surface of target object and then learned a pairwise mapping between the 3D data. Nie[21] further explored the main differences and impacts between cutting edges and removing faces in the topology modification operations in TMN [24].

### 2.2 Metrics in 3D Reconstruction

Chamfer distance [2], Earth Mover Distance (EMD) [27] and Intersection over Union (IoU) are widely-adopted metrics in current researches to measure the distance between reconstructed mesh

and the target object point set. However IoU is not differentiable, so most works use CD and EMD as the loss function of deep learning models as well as metrics to evaluate the quality of reconstructed mesh [6, 11, 12, 21, 37, 42]. CD calculates the nearest pair-wise distance from point set to the other one, while EMD relies on solving an optimization problem to obtain the best mapping function from one set to the other set. Although EMD is more rational than CD, the computation cost of CD is  $O(N \times \log(N))$ , which is much smaller than  $O(N^3 \times \log(N))$  [29] of EMD. In addition, CD can be calculated in parallel and can be further accelerated by KD-tree [3] or Octree [18]. Besides CD and EMD, DPDist [33] and the sliced Wasserstein distance [4] are also proposed in recent years, but they are inconvenient and unstable for various tasks. Thus, we focus on the preferable CD and improve it in the model training and quality evaluation.

### 2.3 Chamfer Distance

Some severe problems have been identified for the metric of CD. For instance, Achlioptas et al. discover that CD is prone to generate outputs with points crowded in the area with highest probability of occupancy (e.g. the seat of chairs), and there exists the imbalance problem between two summands  $CD_{S_1}$  and  $CD_{S_2}$  [1]. Li shows that CD suffers from the local optimum problem in the nearest neighbor search of a finger moving example [14]. In [13], Jin shows that thickening, elongating or shortening four legs of chair results in larger CD values than removing any leg, which implies that CD is not faithful visually and structurally. By comparing the loss of CD and Mean Squared Error (MSE) during training, Wagner et al. find that optimizing CD directly will neglect some details especially for densely sampled point cloud [34]. Paschalidou [25] points out that the CD optimized Atlasnet [12] will predict meshes with zero volume primitives and inverted normals, this is also evidence of self-intersection caused by CD.

Meanwhile, some variant CDs have been proposed in recent years. Li [14] proposed structured chamfer distance which divides 3D objects into several regions and computes the nearest neighbour search in a region-to-region manner other than all-to-all manner. However, this pre-segmentation is time-consuming and still faces the same CD problems in most regions. Lim [16] provided a sharper version of CD, which summarizes the  $p$  power of each distance over all the points and then computes its  $p$ -th root. Their scheme punishes points with larger errors more heavily than before. Wang [35] proposed an adaptive Chamfer loss for better aligning partial shapes. In detail, they obtained the overlapping subset for each point set with a pre-defined distance threshold and then applied CD to these two overlapping subsets. In each optimization process, the predefined distance threshold is chosen adaptively. Li [15] presented a probabilistic chamfer loss for accurate key point localization. Chen [7] proposed an augmented CD by only choosing the largest term each time. A closely related work is [39]. In [39], Wu proposed a Density-aware CD (DCD) for balanced point cloud reconstruction. DCD considers each vertex equally in terms of its queried frequency and then lessens the impact of outliers. In comparison, our work concentrates on mesh reconstruction and its IT and VC problems. We start from a novel point of view by synchronizing the deformation points with a moderate speed and correct direction. In sum, our target problem, main techniques, and evaluation metrics all differ [39].

Some auxiliary constraints are added to CD loss function to improve local details of mesh. These auxiliary metrics include factual auxiliary metrics and hypothetical auxiliary metrics. For the first categories, edge distance [11] avoids merging adjacent edges; Laplacian loss [10] and normal loss [37] both impose the smoothness of mesh; boundary regularization [24] enforces smoothness and consistency of boundary curves; and locality loss [16] penalizes points which locates outside of a small spatial region. For the second group of auxiliary metrics, unup3d [38] assumes that all human faces are symmetric on the whole. Alex [5] studied how the physics-inspired priors influence the model's ability to learn dynamics, with the hypothesis that all real-world video datasets are

Table 1. Notations frequently used in this paper

Notations	Explanations
$S_1$	The ground truth point set of 3D object
$S_2$	The vertex set of synthetic mesh
$V_i$	The $i$ -th vertex in the mesh set $S_2$
$P_j$	The $j$ -th point of the ground truth point set $S_1$
$\phi(V_i)$	$V_i$ 's nearest point in $S_1$
$\psi(P_j)$	$P_j$ 's nearest vertex in $S_2$
$\mathbb{P}_{V_i}$	Points in $S_1$ whose nearest vertex in $S_2$ is $V_i$
$\mathbb{V}_{P_j}$	Vertices in $S_2$ whose nearest point in $S_1$ is $P_j$

governed by the law of physics. Michael [22] argued that deep learning based methods cannot survive without prior knowledge. Finally, most auxiliary constraints are orthogonal to our paper, and auxiliary metrics are not the focus of this paper.

### 3 PROBLEM STATEMENT AND ANALYSIS

#### 3.1 Chamfer Distance

Chamfer Distance (CD), proposed by Barrow et al. in [2], is a commonly-used metric to measure the pair-wise average nearest distance between two point sets. In deep learning model of 3D mesh reconstruction, CD is chosen as the loss function in the optimization process and the evaluation metric of 3D mesh quality. Mathematically, CD is defined as

$$d_{CD}(S_1, S_2) = \frac{1}{|S_1|} \sum_{x \in S_1} \min_{y \in S_2} \|x - y\|_2^2 + \frac{1}{|S_2|} \sum_{y \in S_2} \min_{x \in S_1} \|x - y\|_2^2,$$

where  $S_1 \subseteq \mathbb{R}^3$  is the ground truth point set and  $S_2 \subseteq \mathbb{R}^3$  is the reconstructed mesh vertex set<sup>1</sup>. The calculation of CD is composed of two components  $d_{CD1}$  and  $d_{CD2}$ . The term  $d_{CD1}$  considers the average nearest distance to vertices in  $S_2$  for points in the ground truth set  $S_1$ , while the second term  $d_{CD2}$  evaluates the average nearest distance to the  $S_1$  for vertices in mesh  $S_2$ .

In most scenarios, we have  $|S_1| \gg |S_2|$ . For instance, each ground truth 3D object consists of 10,000 points in Pix3D dataset [21], and 30,000 points in ShapeNet [6], while the sphere template for deformation only use 2,562 vertices in both Total3D[21] and Atlanset[12] due to limitations of computing resources. This implies limited vertices should be used evenly and efficiently to model the target object. In other words, meshes with VC and IT problems waste some vertices and have deficient information about ground truth objects, which further hinders the application of mesh models. For simplicity, we list some commonly-used notations in Table 1.

#### 3.2 Toy Example of VC and IT Problems

In this subsection, we provide a toy example to demonstrate the mesh deformation process with CD loss in Fig. 2. In this example, we use 81 pink dots (ground-truth set  $S_1$ ) to describe the side view of a wooden chair and 40 purple triangle\_right with edges denoted by blue line to represent a mesh template set  $S_2$ . We first calculate CD between these two sets and use `API torch.Tensor.backward()` in PyTorch to obtain the gradient of each vertex denoted by the cyan line with arrow. Then, we move each vertex of mesh, following the magnitude and direction of its gradient. This process

<sup>1</sup>For explicitly description, we use the term vertex to denote point in the reconstructed mesh.

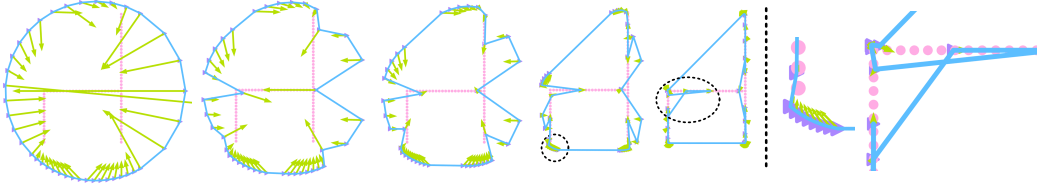


Fig. 2. A toy 2D chair deformation example and details of VC and IT problems. Deformation gradients are provided by CD, pink dot: points of ground truth  $toyS_1$ , purple triangle\_right: mesh vertices  $toyS_2$ , blue line: edges between vertices, cyan arrow: gradient of mesh vertex, on the right: magnified VC and IT problems in dotted circles.

iterates until CD loss cannot be decreased. Some snapshots of this process are shown in Fig. 2, we also provide the magnified VC and IT problems in dotted circles.

From Fig. 2, we have two observations. (1) Some vertices in  $S_2$  approach the end of chair legs and back. The deformation with CD loss makes the excessive number of vertices crowd in a small region, which wastes vertices to model other parts like the cushion surface of chair. We explicitly present these over-crowded vertices with dotted circles in the right sub-figure of Fig. 2 and call these problems of deformation by Vertices Clustering (VC). (2) Other vertices rush into the interior of chair cushion. Actually, no vertex inside of cushion is needed and it is the best practice to use enough vertices to describe the surface of cushion. In 3D deformation process, this aggressive stepping of these vertices generates the unexpected twist of faces. We can also find this problem in 2D cases with a useless line in the fifth sub-figure of Fig. 2. These phenomena cause the generated mesh not to properly align with the target object. We name this problem Illogical Twisting (IT). Both VC and IT problems are induced by CD which only pursues the point level similarly in the brute-force nearest neighbour search, ignoring the edge relations of the mesh and the overall shape of the target object.

### 3.3 Definition of VC and IT Problems

**VC Problem.** Vertices Clustering (VC) describes the scenario where multiple vertices of  $S_2$  crowd and overlap with each other in a small region of a few points in  $S_1$ . We provide the formal definition of VC as follows:

**DEFINITION 1.** *Vertices Clustering: Let  $\bar{d}(S_1)$  be the average distance between points in  $S_1$ , and define the distance threshold between two vertices in  $S_2$  as  $\sigma_{VC} = \rho\bar{d}(S_1)$ , where the coefficient  $\rho$  is a hyper-parameter. Then, we have two criteria to evaluate VC problem: (1) the size  $N_{VC}$  of VC vertices set  $S_{VC} \subseteq S_2$ , where each vertex has the nearest neighbor with the distance smaller than  $\sigma_{VC}$  ( $d(V_i, V_j) < \sigma_{VC}$ ); and (2) the number of vertices  $N_{VC}$ , which has both the nearest neighbor in  $S_2$  with distance smaller than  $\sigma_{VC}$  and identical nearest points in  $S_1$  ( $d(V_i, V_j) < \sigma_{VC}$  &  $\phi(V_i) = \phi(V_j)$ ).*

From the above definition, we argue that VC endeavours to find those mesh vertices that are extremely close to each other, which is not desired during deformation. The goal of mesh deformation is to evenly distribute vertices over the surface of the target 3D object. Furthermore, we can use this core idea of this definition to design a fine-grained deformation scheme, which imperatively distributes mesh vertices in the deformation process. Finally, two criteria of VC can be used as the quality evaluation metric of synthetic mesh as well.

In the existing CD-based schemes, VC problem universally exists, evaluating with the metric in the above definition. In Table 4, we use the results of Atlasnet [12] to exemplify the VC problem. We can find that the classes of rifle, lamp and airplane are prone to have VC problems. For rifle

object, there are 367 VC vertices of the first type (i.e.,  $N_{VC} = 367$ ) among 2562 total vertices and 314 VC vertices of the second type (i.e.,  $N_{VC} = 314$ ), when  $\rho = 0.25$  in the following experiments. The average percentage of first type VC metrics ( $N_{VC}/|S_2|$ ) and second type of VC metrics ( $N_{VC}/|S_2|$ ) are separately 14.3% and 12.3% for the class of ruffle. We can also find that our proposed scheme CD<sup>2</sup> can drastically reduce the number of VC vertex.

**IT Problem.** Illogical Twisting (IT) problem refers to the situation where some parts of a mesh intersect with itself or rush into the inner region as shown in Fig. 1. The IT problem can also be formally defined as follows:

**DEFINITION 2.** *Illegal Twist: For any two faces  $f_i$  and  $f_j$ , let  $v(f_i, f_j)$  denote the number of shared vertices between these two faces. If  $v(f_i, f_j) = 0$ , we use the algorithm in [41] to determine whether  $f_i$  intersects with  $f_j$  or not and construct a IT face set  $S_{IT}$  with this algorithm. Then, we have two criteria to evaluate IT problem: (1) the size of IT face set  $F_{IT} = |S_{IT}|$ ; and (2) the number for vertices  $V_{IT}$  which belong to those faces in  $S_{IT}$ .*

The IT phenomenon occurs universally in the reconstructed mesh of Atlasnet in Fig. 5 (yellow marked faces) and Total3D in Fig. 6 (top view of the bed). Besides the visual results, we can also use two types of IT metrics to evaluate the results of Atlasnet in Table 4. From this table, it can be easily found that the reconstructed meshes of table, ruffle, chair, and bench have severe IT problems. For the class of table, there exist 809.5 IT faces of first type IT metrics on average and 677.8 vertices of the second type of IT metrics. The percentages are separately 15.8% and 26.5%. Although these metrics seem not to be astonishing, these faces and vertices yield an unacceptable and worthless mesh model with obvious and illogical twists which do restrain the mesh from being applied to downstream tasks.

In most cases, ground-truth points are uniformly distributed in datasets and uniformly sampled from datasets, training images with asymmetric objects and distinct confidence leads to unreasonable gradient directions and a huge deformation velocity gap. In other words, visible parts of image have a larger deformation gradient than the invisible parts. Even worse, these excessively-deformed vertices still have large deformation velocity after arriving at the target position and cannot stop moving due to the brute-force nearest neighbour search of CD, as shown in Fig. 2. This over-deformation ultimately results in the intersection and twist of mesh faces. Thus, an intuitive method to identify IT is to find the intersected faces with the existing method. Furthermore, our experiments show that the same number of IT faces may have a different number of vertices, which indicates we can use the vertex number in the intersected faces to evaluate this problem as well. Finally, we should manage the deformation process by orchestrating vertices at an appropriate velocity to prevent the mesh from IT problem.

## 4 METHODS

In this section, we provide two fine-grained schemes called CD<sup>2</sup> both of which compute CD metrics twice in one iteration of mesh deformation. The intuition of CD<sup>2</sup> is to coordinate the vertices of a mesh to perform an appropriate and plausible deformation process, instead of considering vertices equally and moving them aggressively. Our proposed scheme involves two steps. We first calculate the CD metric  $d_{CD}(S_1, S_2)$  to identify some vertices and points and exclude them from further deformation in this round. Then, we compute the CD metric  $d_{CD}(S'_1, S'_2)$  for the residue vertices and points and move these vertices according to gradients obtained from the CD metric  $d_{CD}(S'_1, S'_2)$ .

**Algorithm 1:** Distance-oriented CD<sup>2</sup>


---

**Input:**  $S_1, S_2, p_d, d_T$   
**Output:**  $d_{CD^2}(S_1, S_2)$   
 $Dist_1, Dist_2, index_1, index_2 = d_{CD}(S_1, S_2)$   
 $|S_{2d}| = \max(p_d \times |S_2|, n_t)$   
**for**  $i = 1$  **to**  $|S_2|$  **do**  
    **if**  $Dist_2[i]$  **is top**  $|S_{2d}|$  **smallest then**  
        Append  $S_2[i]$  to  $S_{2d}$   
        Append  $S_1[Index_2[i]]$  to  $S_{1d}$   
    **end**  
**end**  
 $S'_1 = S_1 - S_{1d}$   
 $S'_2 = S_2 - S_{2d}$   
 $Dist'_1, Dist'_2 \leftarrow d_{CD}(S'_1, S'_2)$   
 $d_{CD^2}(S_1, S_2) = Mean(Dist'_1) + Mean(Dist'_2)$

---

**4.1 Distance-oriented CD<sup>2</sup>**

We first present our intuitive but effective scheme called distance-oriented CD<sup>2</sup> which utilized the distance information. Before introducing the exclusion method of vertices in the first step, we present four critical data structures used in the following description as follows:

- $Dist_1$  and  $Index_1$ . For the nearest distance set  $Dist_1$ , the element  $Dist_1[i]$  is the distance from point  $P_i \in S_1$  to its corresponding nearest vertex  $V_j \in S_2$ . We also put the index of this nearest vertex into the set  $Index_1$ , i.e.,  $Index_1[i] = j$ .
- $Dist_2$  and  $Index_2$ . For the nearest distance set  $Dist_2$ , the element  $Dist_2[i]$  is the distance from vertex  $V_i \in S_2$  to its corresponding nearest point  $P_j \in S_1$ . We also put the index of this nearest point into the set  $Index_2$ , i.e.,  $Index_2[i] = j$ .

In the following, we present two methods to identify those aggressive vertices from further deformation. Our first version of CD<sup>2</sup> is to simply exclude those vertices which are extremely close to the ground-truth point set. This idea conforms to the empirical insight that we move all the vertices at a comparable velocity to alleviate various problems. In details, we construct an exclusion vertices set  $S_{2d}$  and its size is determined by two factors, i.e.,  $|S_{2d}| = \max\{[p_d \times |S_2|], n_t\}$ , where the threshold  $p_d \in (0, 1)$  is the percentage of vertices discarded for next CD computation and  $n_t \in (0, |S_2|)$  is the size of vertices whose nearest point distance smaller than the threshold  $d_T$  which we treat as close enough to  $S_1$ . We can easily find those vertices with a certain distance with the data structure  $Dist_1$  and  $Index_1$ . With these two rules, we can construct the vertex set  $S'_2 = S_2 - S_{2d}$ . Meanwhile, we obtain  $S_{1d}$  by mapping the  $S_{2d}$  through  $Index_2$  and obtain the new ground-truth point set  $S'_1$  for further CD computation, this operation is optional. In the following step, we compute the second CD loss for these two set  $S'_1$  and  $S'_2$  and only move vertices in  $S'_2$  to the ground truth points. The detailed algorithm is presented in Algorithm 1.

From Algorithm 1, we can find three potential benefits: (1) Our distance-oriented CD<sup>2</sup> is adaptive, and both vertices and points in each deformation iteration vary according to their distance relationships; (2) The selection of vertex for deformation enable mesh to approach the target 3D object in a synchronization manner, which relieves VC and IT problems; and (3) Although we compute CD twice, the computation cost is not increased too much, since the number of vertex and points are decreased. In addition, our distance-oriented CD<sup>2</sup> still dominates EMD in terms of computation cost, as we will show in Fig. 8.



**Algorithm 2:** Relation-oriented CD<sup>2</sup>


---

**Input:**  $S_1, S_2, pvi_t(pvi_p)$   
**Output:**  $d_{CD^2}(S_1, S_2)$   
 $Dist_1, Dist_2, index_1, index_2 = d_{CD}(S_1, S_2)$   
**for**  $j = 1$  **to**  $|index_1|$  **do**  
     $Pv[index_1[j]] = Pv[index_1[j]] + 1$   
**end**  
**if** *apply*  $CD_t^2$  **then**  
    **for**  $i = 1$  **to**  $|S_2|$  **do**  
        **if**  $Pv[i] > pvi_t$  **then**  
            Append  $S_2[i]$  to  $S_{2d}$   
        **end**  
    **end**  
**end**  
**if** *apply*  $CD_p^2$  **then**  
    **for**  $i = 1$  **to**  $|S_2|$  **do**  
        **if**  $Pv[i]$  *is top*  $pvi_p$  *largest* **then**  
            Append  $S_2[i]$  to  $S_{2d}$   
        **end**  
    **end**  
**end**  
 $S'_2 = S_2 - S_{2d}$   
 $Dist'_1, Dist'_2 = d_{CD}(S_1, S'_2)$   
 $d_{CD^2}(S_1, S_2) = Mean(Dist'_1) + Mean(Dist'_2)$

---

**4.2 Mapping-oriented CD<sup>2</sup>**

Besides the distance information between the mesh vertex set  $S_2$  and ground-truth point set  $S_1$ , additional information on mapping relation can be utilized to orchestrate the deformation process. In the following, we present an improved version of CD<sup>2</sup> based on the points mapping information. Initially, we define a new data structure  $\mathbb{P}_{V_i}$ , which is consisted of a set of points who treat the identical  $V_i$  as their nearest vertex in  $S_2$  ( $\forall P_l \in \mathbb{P}_{V_i}, \psi(P_l) = V_i$ ). The large size of  $\mathbb{P}_{V_i}$  indicates that vertex  $V_i$  is extremely close to the target object, which is not appreciated in mesh deformation. We iterate that all the vertices of mesh should move at a comparable velocity and finally spread evenly around the object surface.

We use  $|\mathbb{P}_{V_i}|$  to exclude some vertices and guide the model learning. In this paper, we provide two specific exclusion methods with vertex-point mapping relation information. One approach called  $CD_t^2$  eliminates vertices whose  $|\mathbb{P}_{V_i}|$  is larger than a predefined threshold( $pvi_t$ ), while the other approach called  $CD_p^2$  just eliminates a certain percentage  $pvi_p$  of vertices with largest  $|\mathbb{P}_{V_i}|$  value. Similarly, we can also delete points according to their  $|\mathbb{V}_{P_j}|$  in  $S_1$ . Then, we remove these vertices from  $S_2$  and move the left vertices to the ground-truth object in the next CD calculation. This vertex-point mapping concerned  $|\mathbb{P}_{V_i}|$  can not only guide the training of a deep learning model but can also be applied to measure the quality of a well-trained model, by count the number of vertices  $V_i$  which have various  $|\mathbb{V}_{P_j}|$ , we can get statistical information on the synthetic meshes which we denote as DPVI as shown in Table 2. The details of our methods are presented in Algorithm 2, for brevity, we only delete  $S_2$  in it.

We show the schematic diagram of traditional CD and our  $CD^2$ ,  $CD_t^2$  ( $pvi_t=1.5$ ) in Fig. 3.

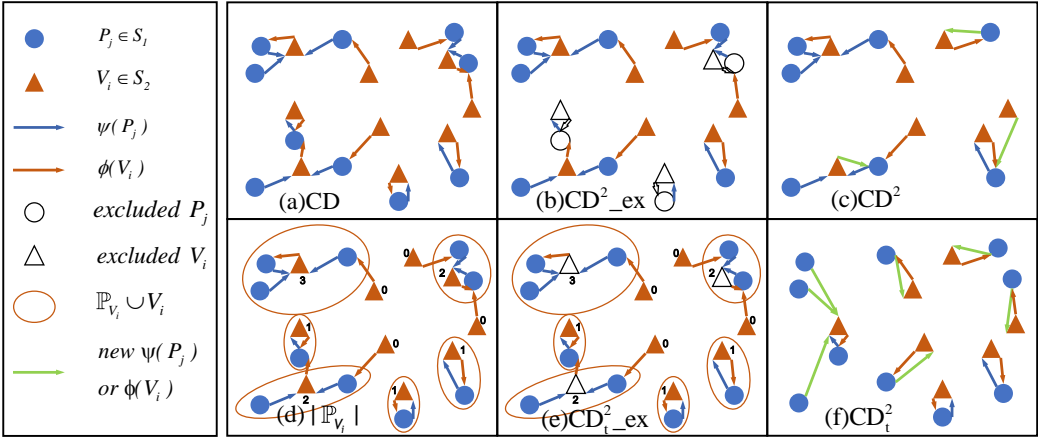


Fig. 3. Schematic diagram of CD, Distance-oriented  $CD^2$  and Relation-oriented  $CD_t^2$ . Left column shows the legend, (a) the mapping principle of traditional CD, (b) how we exclude vertices with  $CD^2$ , (c) the mapping relation of  $CD^2$ , (d) how we obtain  $|P_{V_i}|$ , (e) excluded vertices according to  $|P_{V_i}|$ , (f) the mapping relation of  $CD_t^2$  ( $pvi_t=1.5$ ).

## 5 EXPERIMENTS AND EVALUATIONS

In this section, we compare our proposed methods  $CD^2$ ,  $CD_t^2$ ,  $CD_p^2$  with widely employed Chamfer Distance with two representative works (i.e., Total3D [21] on Pix3D dataset [31] and Atlasnet [12] on ShapeNet dataset [6]). These are two works that deform a template sphere directed by CD, and these two datasets both consist of high-quality 3D point cloud and RGB images of the target objects. The detailed experiment settings will be shown in the next two subsections. Our results are shown in terms of visual demonstration and quantitative analyses with a variety of metrics including our proposed mesh quality metrics (i.e.,  $N_{VC}$ ,  $N_{VC'}$ ,  $F_{IT}$ ,  $P_{IT}$  and DPVI). We will show the time consumption of these metrics in the end of the section.

### 5.1 Experiment with Atlasnet on ShapeNet

We first compare the performance of our  $CD^2$  and  $CD_{p&t}^2$  with CD on a famous 3D reconstruction work Atlasnet [12], this work is trained on ShapeNet [6], which contains about 35 thousand manually created and cleaned 3D CAD samples, each sample consists of a polygon mesh and several rendered pictures from different views, including airplane, bench, cabinet, and car, etc. Atlasnet is a 3D surface generating method that represents 3D shape as a collection of parametric surface elements. Though there are 3 modules in Atlasnet, we find that the autoencoder trained decoder in the first stage outputs most well-structured meshes, the subsequent resnet encoder, and single view reconstruction modules all output more shape alike meshes but have worse topological structures for they only pursue a minimum of CD loss, there modules output meshes with zero volume and inverted normals as Paschalidou[25] declared. So we only experiment with the autoencoder module, we choose to output 1 patch of sphere because multiple patches will certainly generate VC and IT problems in our opinion.

We denote the pretrained model provided by the Atlasnet[12] as  $At_{CD}$ , we completely alter chamfer distance in the system with our algorithms in our settings. For  $CD^2$  method, we set the  $p_d$  to be **0.3**,  $d_T$  to be  $10^{-7}$ , and the learning rate is  $10^{-4}$ . For  $CD_t^2$ , we exclude both the vertices and

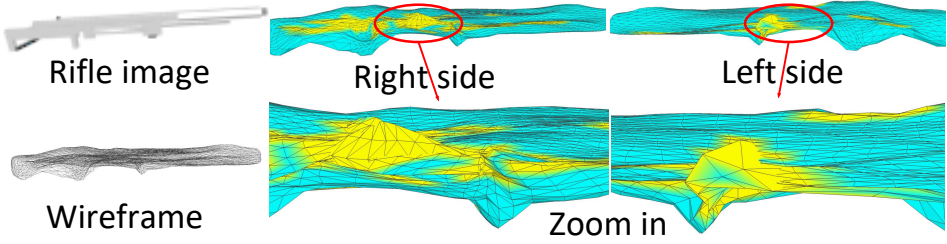


Fig. 4. A rifle mesh produced by  $At_{CD}$

points in  $S_1$  and  $S_2$  with same  $pvi_t$  set as 4, learning rate is also  $10^{-4}$ . For  $CD^2_{pviP}$ , we set  $pvi_p$  to be **0.08** for  $S_2$ , we also exclude the  $S_1$  at the ratio of **0.01**, the learn rate here is also  $10^{-4}$ .

We conduct **visual comparison** using Meshlab[8] here, the results are shown in Fig. 5. The **numerical results** of CD and EMD are presented in Table 3, the CD value is multiplied by  $10^4$ . The statistical results for DPVI are presented in Table 2. The above three values are computed over the entire test set. The comparison of numerical VC and IT problem results is shown in Table 4, we add up the VC value of the first 32 test samples in each category to get the final  $N_{VC}$ , we sum up the IT value of 10 carefully selected samples in each category to get the final  $F_{IT}$  and  $P_{IT}$ , we didn't go through the whole test set for the reason that this two calculation is so time-consuming and the samples for each category only appear several similar shapes and surfaces, we already cover these primary shapes. In all tables, we bold the best result of each category for each numerical metric within these 4 settings. We also randomly select 2562 points from the 30,000 ground truth points to measure the Optimum Performance Theoretically Attainable (OPTA) of CD, EDM, and DPVI.

From the visual and numerical comparison results we have the following findings:

- $CD^2_{p&t}$  perform best in all aspects except CD,  $CD^2$  performs worst in CD, EMD, and VC, while  $At_{CD}$  performs best in CD and worst in remaining aspects.
- Our  $CD^2_{p&t}$  surpass  $At_{CD}$  both in visual and numerical comparison except CD, which proves that CD is not faithful in terms of visual quality. Further, EMD and our proposed VC, IT and DPVI can better mirror the visual and structure quality typically for wireframe of mesh.
- For simply-shaped objects such as car and sofa, our  $CD^2_{p&t}$  can generate meshes with little or no VC or IT problem, these meshes are almost perfect. While  $At_{CD}$  still have IT in illogical parts of mesh on account of the defects of CD, as presented in the first row of Fig. 5.
- All these 4 methods generate meshes with serious IT problems for airplane because the system can only twist the sphere inexplicably to shape the wing and stabilizer for a typical airplane shape, as shown in the first column in Fig. 5, which means these airplane meshes can hardly be applied in downstream tasks. Even so, our  $CD^2_p$  and  $CD^2_t$  are still superior to  $At_{CD}$  in relation to IT.
- $At_{CD}$  generate rifles with a good CD value but with bad VC and IT results, which is because rifle is very small in size, the model just distorts the mesh into a stick-like mess (as shown in Fig. 4) and will obtain fine CD outcome. EMD also fails to discover this mess. However, this distortion is sensed by IT and VC as these two values of rifle are almost the maximum in each method among all classes.
- The stick-like distortion also happens in the lamp, table, chair, bench, and display, due to they have thin stick-like parts, as shown by IT outcomes in Table 4.
- $CD^2$  performs badly in  $|\mathbb{P}_{V_i}|$ , VC and EMD but still has fine IT and visual results, this is because it generates meshes with extremely uneven vertex distribution, these meshes have

vertices at a very high density in parts of it, which is obvious in sofa and vessel in Fig. 5, this leads to the bad outcome of DPVI, VC and EMD, for these three metrics is more density sensitive.

- $CD_p^2$  overwhelms  $CD_t^2$  in VC and IT, which shows the threshold exclusion manner performs better than a fixed proportion manner, for the former is more adaptive during training.
- $CD^2$  is inferior to  $CD_{p\&t}^2$ , which demonstrates that point-vertex mapping relation ( $|\mathbb{P}_{V_i}|$ ) is more important than distance relation ( $Dist[i]$ ) for a more sensible deformation process, in line with the view of Wu[39] to some extent.
- Our  $CD_{p\&t}^2$  produces meshes that have very close EMD values to the OPTA as shown in Table 3, such as cabinet, louder speaker, sofa and telephone, this also verifies the efficiency of our proposal.

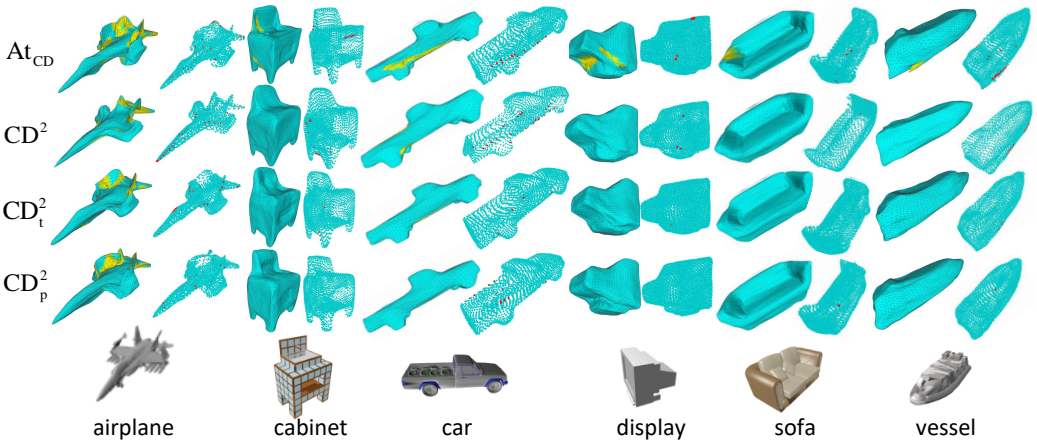


Fig. 5. Meshes on Atlasnet. Rows from top to bottom are the outputs from  $At_{CD}$ ,  $CD^2$ ,  $CD_t^2$  and  $CD_p^2$ , the bottom row is the input image. We show the IT faces marked(yellow) meshes in the left column and the VC vertices(red) marked meshes in the right for each input.

Table 2. Statistical result of DPVI on Atlasnet. Add up from all test samples according to the  $|\mathbb{P}_{V_i}|$ , for value 1, larger is better, for value 0 and 3-max, smaller is better, for value 2, closer to OPTA is better.

$ \mathbb{P}_{V_i} $	0	1	2	3-10	11-20	21-30	31-40	41-50	51-max
$At_{CD}$	10110933	6704860	3358112	2261178	11995	907	164	52	43
$CD^2$	10395176	6488772	3231048	2312918	18520	1382	299	82	47
$CD_p^2$	9975519	<b>6782684</b>	3439256	<b>2241421</b>	8625	<b>572</b>	<b>104</b>	36	<b>27</b>
$CD_t^2$	<b>9969614</b>	6780625	<b>3443509</b>	2245607	<b>8144</b>	582	109	<b>27</b>	<b>27</b>
OPTA	9838211	6841758	3481074	2286980	221	0	0	0	0

Table 3. CD and EMD on Atlasnet. All smaller is better.

Method	Metric	airplane	bench	cabinet	car	chair	display	lamp	speaker	rifle	sofa	table	telephone	vessel	all
At <sub>CD</sub>	CD	<b>8.1</b>	<b>10.9</b>	<b>13.5</b>	14.7	<b>14.4</b>	<b>13.5</b>	<b>21.9</b>	<b>20.2</b>	6.0	<b>13.6</b>	<b>13.9</b>	10.4	<b>12.2</b>	<b>13.3</b>
	EMD	52.1	46.3	46.9	52.1	59.2	57.2	166.0	56.1	63.9	39.5	67.4	53.9	61.9	63.3
CD <sup>2</sup>	CD	9.6	12.4	14.1	16.5	16.2	14.6	25.6	21.5	7.1	14.4	15.9	10.8	14.2	14.8
	EMD	108.6	176.9	165.2	93.1	108.6	164.3	189.8	178.7	79.8	244.8	158.7	75.2	116.3	143.1
CD <sup>2</sup> <sub>t</sub>	CD	8.6	11.3	13.5	14.7	14.9	14.0	23.8	20.5	6.3	13.5	14.6	10.3	13.1	13.8
	EMD	<b>33.8</b>	<b>32.5</b>	31.1	<b>29.2</b>	40.3	34.4	<b>82.0</b>	38.3	50.9	30.2	41.4	27.7	<b>38.4</b>	39.3
CD <sup>2</sup> <sub>p</sub>	CD	8.4	10.9	13.5	<b>14.5</b>	14.6	13.8	22.7	20.2	<b>6.0</b>	13.5	14.1	<b>10.3</b>	12.7	13.5
	EMD	41.0	33.2	<b>30.2</b>	31.0	<b>37.4</b>	<b>32.7</b>	83.7	<b>36.6</b>	<b>46.3</b>	<b>29.6</b>	<b>38.5</b>	<b>26.9</b>	38.5	<b>38.9</b>
OPTA	CD	4.3	6.7	11.6	11.1	9.2	9.5	5.0	13.6	2.3	10.6	8.9	9.2	5.4	8.3
	EMD	17.1	21.3	32.1	26.8	25.6	24.3	20.1	34.0	11.0	26.0	26.1	23.3	15.9	23.4

Table 4. Quantified VC and IT problems results on Atlasnet. Columns except the last represent the average quantity of each sample, the last column is the average percent of these two problems of one sample, each sample consists of 2,562 vertices and 5,120 faces, all less is better.

Method	Metric	airplane	bench	cabinet	car	chair	display	lamp	speaker	rifle	sofa	table	telephone	vessel	Avg.%
At <sub>CD</sub>	$N_{VC}$	188.9	167.7	30.5	30.2	80.9	43.6	257.2	38.9	367.2	35.8	130.6	35.5	142.6	4.7
	$N_{VC'}$	149.9	135.9	23.7	24.1	64.6	35.4	239.4	33.6	314.3	28.6	106.3	25.4	118.9	3.9
	$F_{IT}$	321.0	337.3	74.2	142.9	343.5	213.6	229.9	2.7	<b>486.7</b>	110.1	809.5	60.0	172.2	5.0
	$V_{IT}$	313.1	320.1	81.2	138.2	310.1	189.7	232.5	4.0	<b>450.5</b>	113.5	677.8	77.0	163.8	9.2
CD <sup>2</sup>	$N_{VC}$	357.1	329.5	72.9	44.7	117.5	162.5	242.9	57.9	383.9	115.0	235.5	121.9	166.8	7.2
	$N_{VC'}$	299.7	290.2	58.7	36.5	96.5	138.7	220.0	50.3	342.3	91.8	200.5	92.7	141.2	6.2
	$F_{IT}$	327.7	424.1	96.5	46.7	347.7	176.2	169.7	15.3	631.9	73.5	530.2	59.0	<b>55.5</b>	4.4
	$V_{IT}$	336.6	407.6	100.7	46.5	311.4	184.7	188.4	20.0	600.8	77.9	502.5	69.1	<b>69.7</b>	8.8
CD <sup>2</sup> <sub>t</sub>	$N_{VC}$	<b>182.3</b>	<b>156.5</b>	<b>20.1</b>	7.9	<b>67.4</b>	<b>42.5</b>	<b>120.1</b>	<b>21.1</b>	<b>213.1</b>	<b>27.4</b>	<b>114.6</b>	<b>29.1</b>	83.1	<b>3.3</b>
	$N_{VC'}$	<b>145.3</b>	<b>126.9</b>	<b>15.2</b>	6.1	<b>55.8</b>	<b>33.5</b>	<b>102.6</b>	<b>17.6</b>	<b>178.9</b>	<b>20.8</b>	<b>92.5</b>	<b>20.8</b>	66.8	<b>2.6</b>
	$F_{IT}$	<b>233.1</b>	<b>265.6</b>	<b>61.9</b>	12.7	<b>189.5</b>	<b>137.3</b>	<b>167.2</b>	2.6	<b>759.7</b>	70.3	<b>462.4</b>	<b>46.4</b>	152.2	<b>3.8</b>
	$V_{IT}$	<b>250.7</b>	<b>249.8</b>	<b>63.2</b>	<b>13.9</b>	<b>184.7</b>	<b>137.9</b>	<b>179.2</b>	<b>4.1</b>	<b>680.2</b>	75.8	<b>444.2</b>	<b>54.2</b>	148.2	7.5
CD <sup>2</sup> <sub>p</sub>	$N_{VC}$	223.2	193.3	28.9	22.6	90.7	54.8	147.5	30.9	233.1	31.8	123.8	37.1	<b>72.8</b>	3.9
	$N_{VC'}$	181.2	158.5	22.4	17.4	75.1	42.2	129.5	25.1	194.6	25.9	101.1	28.9	<b>58.1</b>	3.2
	$F_{IT}$	285.8	300.2	86.4	26.4	293.0	233.5	187.9	<b>2.1</b>	601.6	<b>59.3</b>	529.5	59.0	96.9	4.1
	$V_{IT}$	299.8	296.9	86.3	32.2	283.2	209.5	195.7	<b>3.6</b>	537.4	<b>63.6</b>	474.9	60.8	97.4	7.9

## 5.2 Experiment with Total3D on Pix3D

The state-of-art work Total3D[21] studies 3D indoor reconstruction and scene understanding task and achieves less mean CD value on Pix3D dataset than other famous results[7, 12]. Pix3D is a large-scale dataset of well aligned 2D images and 3D shapes, and it consists of 10,069 image-shape pairs from 395 different indoor furniture with 9 categories. In this paper, we provides several Total3D models, i.e, an completed model T3d<sub>pre</sub> provided by Nie[21], and a original T3D<sub>CD</sub> trained from scratch without any pretrained model, and two settings trained by our CD<sup>2</sup> and CD<sup>2</sup><sub>t</sub>. In our CD<sup>2</sup> setting, we set the hyper-parameter  $p_{del} = 0.6$  and  $d_T = 0$ , learning rate  $10^{-4}$ , we do exclude  $S_1$  here. In CD<sup>2</sup><sub>t</sub> setting, the  $p_{vit}$  is 4, learning rate is  $10^{-5}$ , we only exclude  $S_2$  here. The train-test split is adopted as [11] for all three models, and we use object label mapping from NYU-37 [30].

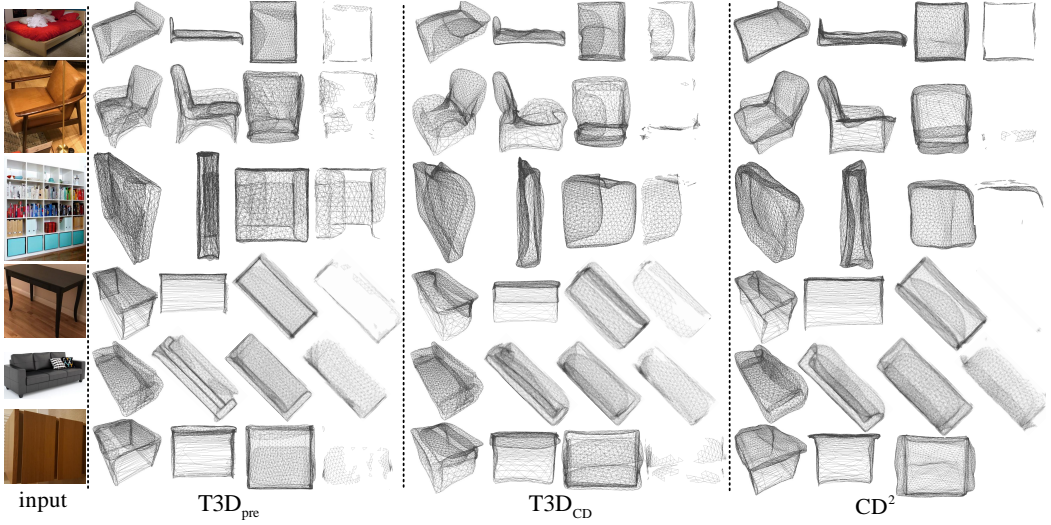


Fig. 6. Meshes on Total3D. From left to right, the RGB image input from Pix3D, wireframes of meshes from three different views and the invisible faces of the column close on the left, meshes are from three methods:  $T3D_{pre}$ ,  $T3D_{CD}$ ,  $CD^2$ . From top to bottom are image and corresponding meshes of bed, chair, bookcase, desk, sofa and table.

We first present the **visual comparisons** of six classes of Pix3D from different views in Fig. 6, which are produced by  $T3D_{pre}$ ,  $T3D_{CD}$  and  $CD^2$ . We render these meshes by ‘GLC\_Player’ here. We can easily find that meshes produced by  $T3D_{pre}$  and  $T3D_{CD}$  have IT and VC problems from their wireframes. For example, beds have an obvious fold in the left part in row 1; chairs also have some faces folded into cushions in row 2, bookcase in row 3, and tables in row 6 have twists inside the shelf and desktop. These twists are illogical and useless. Fortunately, our  $CD^2$  produces meshes with much fewer twists in most classes, especially for bed, the structure of mesh generated by our  $CD^2$  is also more sensible than  $T3D_{pre}$ . Although meshes of sofa and table generated by our scheme are not satisfying and have apparent structure problems, these meshes are still much better than the other CD-based settings.

The last columns of each method in Fig. 6 are the invisible faces of the meshes that remained after deleting all visible faces, this is done with the “select Faces in a rectangular region” and “select only visible” functions in MeshLab[8], we rotate the mesh  $S_2$  a dozen times randomly and select and repeat the above operation, then we delete all the selected faces and obtain the remained faces. We can find that even  $T3D_{CD}$  create surface similar meshes, the invisible faces in the interior of these meshes are at a significant quantity and form illogical shapes, this happens more serious for bed, chair, bookcase, and table. But when it comes to our  $CD^2$ , the synthetic meshes have the least invisible faces except for sofa, we even have no invisible faces for table. These findings can mirror the well structural quality of our meshes for more faces contribute to forming the details of the target 3D object.

For **mathematical comparison**, we conduct on three methods: the offered  $T3D_{pre}$ , our  $CD^2$  and  $CD^2_t$ . We show the IT and VC results on Total3D in Table 5, this experiment also demonstrates that our  $CD^2_t$  performs better than  $T3D_{pre}$ , especially for IT problem,  $T3D_{pre}$  outputs meshes with more than a quarter(28.10%) of all faces and nearly half(46.44%) of all vertices have IT problems.

Table 5. Quantified VC and IT problems results on Total3D. Columns except the last represent the average quantity of each sample, the last column is the average percent of these two problems of one sample by treating each category equal, one sample consists of 2,562 vertices and 5,120 faces, all less is better.

Method	Metric	bed	bookcase	chair	desk	msic	sofa	table	tools	wardrobe	Avg.%
T3D <sub>pre</sub>	Nvc	263.3	523.7	<b>489.5</b>	<b>644.8</b>	440.5	180.3	<b>347.9</b>	461.5	<b>190.9</b>	15.36
	Nvc'	200.0	446.5	<b>423.2</b>	<b>559.8</b>	381.8	129.4	<b>285.0</b>	403.7	<b>149.2</b>	12.92
	Fit	893.1	1265.5	1549.5	2283.0	1334.4	777.6	1429.5	2834.2	581.9	28.10
	Vit	830.1	1174.7	1281.9	1763.6	1133.5	729.8	1211.9	2054.7	528.9	46.44
CD <sup>2</sup>	Nvc	464.8	892.4	923.0	1051.6	574.9	228.8	731.6	500.8	322.8	24.68
	Nvc'	389.2	816.2	832.1	974.8	520.9	174.5	630.6	431.5	259.7	21.81
	Fit	909.6	1195.7	1479.4	1777.6	682.5	838.0	1238.4	1858.6	511.8	22.77
	Vit	860.4	1001.3	1243.9	1484.5	648.2	809.0	1053.6	1445.2	497.9	39.22
CD <sub>t</sub> <sup>2</sup>	Nvc	<b>148.0</b>	<b>456.5</b>	590.5	671.7	<b>175.5</b>	<b>74.7</b>	526.4	<b>151.8</b>	287.8	<b>13.37</b>
	Nvc'	<b>121.2</b>	<b>419.1</b>	521.8	610.8	<b>152.4</b>	<b>58.1</b>	459.3	<b>124.7</b>	243.5	<b>11.76</b>
	Fit	<b>344.4</b>	<b>642.2</b>	<b>941.9</b>	<b>1351.2</b>	<b>351.5</b>	<b>275.8</b>	<b>725.9</b>	<b>1002.0</b>	<b>392.7</b>	<b>13.08</b>
	Vit	<b>356.4</b>	<b>560.9</b>	<b>867.6</b>	<b>1171.4</b>	<b>352.3</b>	<b>285.7</b>	<b>678.7</b>	<b>946.4</b>	<b>381.3</b>	<b>24.29</b>

Table 6. EMD results on Total3D. All is divided by 100, the last average column is the mean of each category, all smaller is better.

	bed	bookcase	chair	desk	msic	sofa	table	tools	wardrobe	Avg
T3D <sub>pre</sub>	<b>2.71</b>	12.88	<b>4.81</b>	<b>5.98</b>	<b>11.69</b>	2.14	<b>6.52</b>	<b>13.67</b>	7.42	7.54
CD <sup>2</sup>	<b>3.64</b>	11.72	8.00	<b>7.94</b>	10.84	<b>1.88</b>	6.55	<b>8.33</b>	<b>2.89</b>	6.87
CD <sub>t</sub> <sup>2</sup>	3.85	<b>9.99</b>	6.07	6.42	<b>10.30</b>	2.24	6.89	8.95	4.86	<b>6.62</b>

Table 7. Quantity of invisible faces of generated meshes. Less is better.

Method	Bed	Bookcase	Chair	Desk&Table	Sofa
T3D <sub>pre</sub>	604	890.6	473.8	377.8	1071.7
T3D <sub>CD</sub>	979	1023.4	499.2	428.4	1307.7
CD <sup>2</sup>	310	386.8	139	17.2	1081

But the IT-related faces of our CD<sub>t</sub><sup>2</sup> are obly half of the T3D<sub>pre</sub>. In addition, our CD<sub>t</sub><sup>2</sup> prevails over CD<sup>2</sup> again, which is also consistent with the previous result of Atlasnet in Sec. 5.1.

We show the EMD result on Total3D with the T3d<sub>pre</sub>, our CD<sup>2</sup> and CD<sub>t</sub><sup>2</sup>, we achieve better EMD results than the CD based T3d<sub>pre</sub>, as shown in Table 6. The T3d<sub>pre</sub> has best CD results of all categories which we treat as unreliable, so we don't show the CD results in this paper.

We also randomly select 10 samples from some category and calculate the mean of the number of invisible faces in Table 7, the meshes produced by CD<sup>2</sup> have evident fewer invisible faces than T3D<sub>CD</sub> and T3D<sub>pre</sub> except for sofa, which proves that meshes generated by CD<sup>2</sup> have a greater percentage of faces contributing to the real sense of surface, and these meshes are more informative and well-structured than CD-based methods, this also proves the benefit of our proposal.

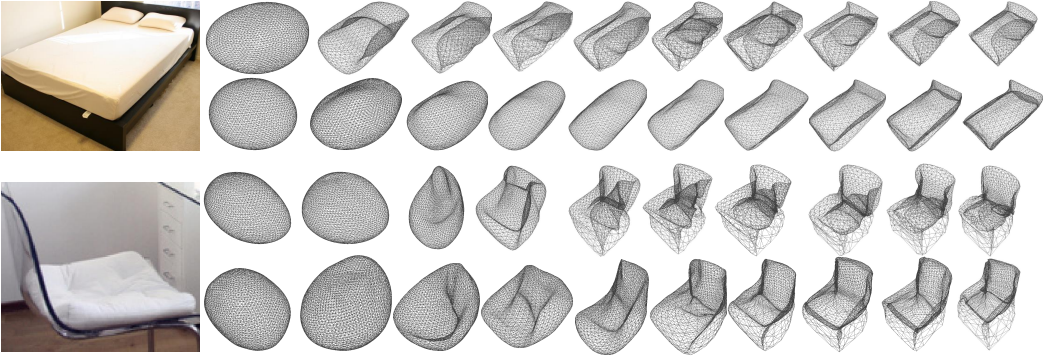


Fig. 7. Meshes produced during learning progress. From left to right, the RGB image input, meshes produced in different training epochs. From top to bottom, meshes of bed produced by  $T3D_{CD}$  (row 1) and  $CD^2$  (row 2), meshes of chair produced by  $T3D_{CD}$  (row 3) and  $CD^2$  (row 4).

Besides the ultimate meshes, we demonstrate the deformation process of two samples in Fig. 7. In rows 1 and row 3, we can see the generation of folds and twists caused by the CD in this Total3D[21]. However, our  $CD^2$  in row 2 and row 4 succeeds in approaching the target object by performing the adaptive choice of vertices or points in each deform epoch. We abandon the brute-force nearest neighbour search and minimal gradient procedure but succeed in realizing more intuitive and sensible deformation progress, and output more well-structured and workable meshes at last. Fig. 7 is a crucial proof of the efficiency of our  $CD^2$ .

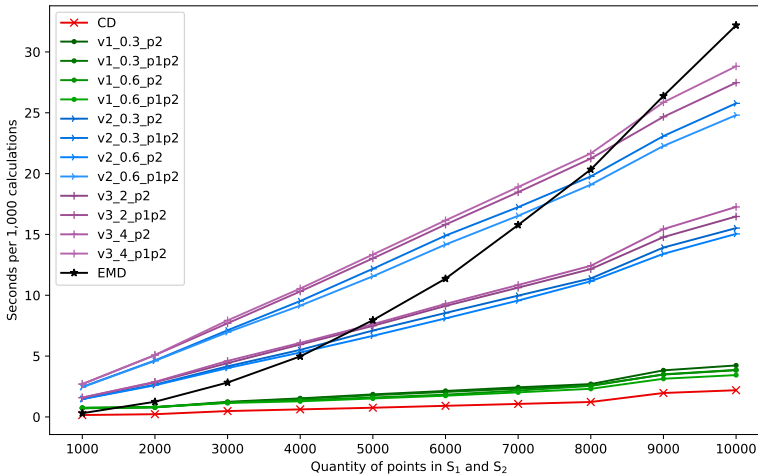


Fig. 8. Time consumption of CD, EMD, and  $CD^2$ s. The value of EMD is divided by 45 in order to be shown in one figure, v1 means  $CD^2$ , v2 means  $CD^2_p$ , v3 means  $CD^2_t$ , the following decimals means the exclusion percentage ( $p_d$  and  $p_{vi_p}$ ) and the integers means the exclusion threshold ( $p_{vi_t}$ ), p2 means only exclude  $S_2$  and p1p2 means both exclude  $S_1$  and  $S_2$ .



### 5.3 Time consumption of CD, EMD and CD<sup>2</sup>s

We show the time consumption for three metrics: CD, EMD, and CD<sup>2</sup>s to calculate the distance between two point sets  $S_1$  and  $S_2$  for 1,000 times, the result is shown in Fig.8. We can see that our CD<sup>2</sup> have very close time consumption to CD, CD<sub>p</sub><sup>2</sup> and CD<sub>t</sub><sup>2</sup> have larger slopes because our  $|\mathbb{P}_{V_i}|$ -based vertex eliminate operation do consume more time than distance-based method, but all the time consumption of our metrics is still in the same order of magnitude as CD, they almost increase linearly as the number of points in  $S_1$  and  $S_2$  goes up. However, the EMD has an exponential rise of time consumption, which is much larger than CD-based metrics, when there are 10,000 points in each point set, it needs more than 1,200 seconds for EMD to calculate 1,000 times. So our CD<sup>2</sup>s are both more effective and efficient than EMD.

## 6 CONCLUSION

In this paper, we demonstrate that the Chamfer distance is inadequate for deep learning based monocular 3D mesh reconstruction tasks, and identify that it will produce meshes with Illogical Twists and Vertices Clustering problems, making the outputs hardly able to be applied to downstream tasks. We highlight these drawbacks of CD with detailed visualization comparison as well as the quantified VC and IT data. Then, we present a twice Chamfer distance CD<sup>2</sup> which employs CD twice in one calculation, we further proposed an enhanced CD<sub>p&t</sub><sup>2</sup> based on points-vertex mapping relations. We succeed in generating more sensible meshes in a slowly approaching manner and producing more edge plausible and well-structured meshes on Pix3D and ShapeNet. We demonstrated that the quantified IT and VC data, the statistical results DPVI of  $|\mathbb{P}_{V_i}|$ , in addition to invisible faces, are all faithful manners for better evaluating the practicability of meshes. Our work is promising since our CD<sup>2</sup>s can be easily applied to any 3D reconstruction tasks in the future, it will help obtain better-structured and useful output for further applications.

## REFERENCES

- [1] ACHLIOPTAS, P., DIAMANTI, O., MITLAGKAS, I., AND GUIBAS, L. Learning representations and generative models for 3d point clouds. In *International conference on machine learning* (2018), PMLR, pp. 40–49.
- [2] BARROW, H. G., TENENBAUM, J. M., BOLLES, R. C., AND WOLF, H. C. Parametric correspondence and chamfer matching: Two new techniques for image matching. Tech. rep., SRI INTERNATIONAL MENLO PARK CA ARTIFICIAL INTELLIGENCE CENTER, 1977.
- [3] BENTLEY, J. L. Multidimensional binary search trees used for associative searching. *Communications of the ACM* 18, 9 (Sept. 1975), 509–517.
- [4] BONNEEL, N., RABIN, J., PEYRÉ, G., AND PFISTER, H. Sliced and radon wasserstein barycenters of measures. *Journal of Mathematical Imaging and Vision* 51, 1 (2015), 22–45.
- [5] BOTEV, A., JAEGLER, A., WIRNSBERGER, P., HENNES, D., AND HIGGINS, I. Which priors matter? benchmarking models for learning latent dynamics. *arXiv preprint arXiv:2111.05458* (2021).
- [6] CHANG, A. X., FUNKHOUSER, T., GUIBAS, L., HANRAHAN, P., HUANG, Q., LI, Z., SAVARESE, S., SAVVA, M., SONG, S., SU, H., ET AL. Shapenet: An information-rich 3d model repository. *arXiv preprint arXiv:1512.03012* (2015).
- [7] CHEN, S., DUAN, C., YANG, Y., LI, D., FENG, C., AND TIAN, D. Deep Unsupervised Learning of 3D Point Clouds via Graph Topology Inference and Filtering. *IEEE Transactions on Image Processing* 29 (2020), 3183–3198.
- [8] CIGNONI, P., CALLIERI, M., CORSINI, M., DELLEPIANE, M., GANOVELLI, F., RANZUGLIA, G., ET AL. Meshlab: an open-source mesh processing tool. In *Eurographics Italian chapter conference* (2008), vol. 2008, Salerno, Italy, pp. 129–136.
- [9] DAI, A., QI, C. R., AND NIEBNER, M. Shape Completion Using 3D-Encoder-Predictor CNNs and Shape Synthesis. In *2017 IEEE Conference on Computer Vision and Pattern Recognition (CVPR)* (Honolulu, HI, July 2017), IEEE, pp. 6545–6554.
- [10] DESBRUN, M., MEYER, M., SCHRÖDER, P., AND BARR, A. H. Implicit fairing of irregular meshes using diffusion and curvature flow. In *Proceedings of the 26th annual conference on Computer graphics and interactive techniques - SIGGRAPH '99* (Not Known, 1999), ACM Press, pp. 317–324.
- [11] GKIOXARI, G., JOHNSON, J., AND MALIK, J. Mesh R-CNN. In *2019 IEEE/CVF International Conference on Computer Vision (ICCV)* (Seoul, Korea (South), Oct. 2019), IEEE, pp. 9784–9794.
- [12] GROUEIX, T., FISHER, M., KIM, V. G., RUSSELL, B. C., AND AUBRY, M. A Papier-Mache Approach to Learning 3D Surface Generation. In *2018 IEEE/CVF Conference on Computer Vision and Pattern Recognition* (Salt Lake City, UT, USA, June

- 2018), IEEE, pp. 216–224.
- [13] JIN, J., PATIL, A. G., XIONG, Z., AND ZHANG, H. Dr-kfs: A differentiable visual similarity metric for 3d shape reconstruction. In *European Conference on Computer Vision (2020)*, Springer, pp. 295–311.
  - [14] LI, C.-L., SIMON, T., SARAGI, J., POZOS, B., AND SHEIKH, Y. LBS Autoencoder: Self-Supervised Fitting of Articulated Meshes to Point Clouds. In *2019 IEEE/CVF Conference on Computer Vision and Pattern Recognition (CVPR)* (Long Beach, CA, USA, June 2019), IEEE, pp. 11959–11968.
  - [15] LI, J., AND LEE, G. H. USIP: Unsupervised Stable Interest Point Detection From 3D Point Clouds. In *2019 IEEE/CVF International Conference on Computer Vision (ICCV)* (Seoul, Korea (South), Oct. 2019), IEEE, pp. 361–370.
  - [16] LIM, I., IBING, M., AND KOBELT, L. A Convolutional Decoder for Point Clouds using Adaptive Instance Normalization. *Computer Graphics Forum* 38, 5 (Aug. 2019), 99–108.
  - [17] LIN, C.-H., KONG, C., AND LUCEY, S. Learning efficient point cloud generation for dense 3d object reconstruction. In *proceedings of the AAAI Conference on Artificial Intelligence (2018)*, vol. 32.
  - [18] MEAGHER, D. Octree encoding: A new technique for the representation, manipulation and display of arbitrary 3-d objects by computer.
  - [19] MESCHEDER, L., OECHSLE, M., NIEMEYER, M., NOWOZIN, S., AND GEIGER, A. Occupancy Networks: Learning 3D Reconstruction in Function Space. In *2019 IEEE/CVF Conference on Computer Vision and Pattern Recognition (CVPR)* (Long Beach, CA, USA, June 2019), IEEE, pp. 4455–4465.
  - [20] NGUYEN, D., CHOI, S., KIM, W., AND LEE, S. GraphX-Convolution for Point Cloud Deformation in 2D-to-3D Conversion. In *2019 IEEE/CVF International Conference on Computer Vision (ICCV)* (Seoul, Korea (South), Oct. 2019), IEEE, pp. 8627–8636.
  - [21] NIE, Y., HAN, X., GUO, S., ZHENG, Y., CHANG, J., AND ZHANG, J. J. Total3DUnderstanding: Joint Layout, Object Pose and Mesh Reconstruction for Indoor Scenes From a Single Image. In *2020 IEEE/CVF Conference on Computer Vision and Pattern Recognition (CVPR)* (Seattle, WA, USA, June 2020), IEEE, pp. 52–61.
  - [22] OECHSLE, M., PENG, S., AND GEIGER, A. UNISURF: Unifying Neural Implicit Surfaces and Radiance Fields for Multi-View Reconstruction. In *2021 IEEE/CVF International Conference on Computer Vision (ICCV)* (Montreal, QC, Canada, Oct. 2021), IEEE, pp. 5569–5579.
  - [23] PALA, P., AND BERRETTI, S. Reconstructing 3D Face Models by Incremental Aggregation and Refinement of Depth Frames. *ACM Transactions on Multimedia Computing, Communications, and Applications* 15, 1 (Feb. 2019), 1–24.
  - [24] PAN, J., HAN, X., CHEN, W., TANG, J., AND JIA, K. Deep Mesh Reconstruction From Single RGB Images via Topology Modification Networks. In *2019 IEEE/CVF International Conference on Computer Vision (ICCV)* (Seoul, Korea (South), Oct. 2019), IEEE, pp. 9963–9972.
  - [25] PASCHALIDOU, D., KATHAROPOULOS, A., GEIGER, A., AND FIDLER, S. Neural Parts: Learning Expressive 3D Shape Abstractions with Invertible Neural Networks. In *2021 IEEE/CVF Conference on Computer Vision and Pattern Recognition (CVPR)* (Nashville, TN, USA, June 2021), IEEE, pp. 3203–3214.
  - [26] PONTES, J. K., KONG, C., SRIDHARAN, S., LUCEY, S., ERIKSSON, A., AND FOKES, C. Image2mesh: A learning framework for single image 3d reconstruction. In *Asian Conference on Computer Vision (2018)*, Springer, pp. 365–381.
  - [27] RUBNER, Y., TOMASI, C., AND GUIBAS, L. J. The earth mover’s distance as a metric for image retrieval. *International journal of computer vision* 40, 2 (2000), 99–121.
  - [28] SHIN, D., REN, Z., SUDDERTH, E., AND FOWLKES, C. 3D Scene Reconstruction With Multi-Layer Depth and Epipolar Transformers. In *2019 IEEE/CVF International Conference on Computer Vision (ICCV)* (Seoul, Korea (South), Oct. 2019), IEEE, pp. 2172–2182.
  - [29] SHIRDHONKAR, S., AND JACOBS, D. W. Approximate earth mover’s distance in linear time. In *2008 IEEE Conference on Computer Vision and Pattern Recognition (2008)*, IEEE, pp. 1–8.
  - [30] SILBERMAN, N., HOIEM, D., KOHLI, P., AND FERGUS, R. Indoor segmentation and support inference from rgbd images. In *European conference on computer vision (2012)*, Springer, pp. 746–760.
  - [31] SUN, X., WU, J., ZHANG, X., ZHANG, Z., ZHANG, C., XUE, T., TENENBAUM, J. B., AND FREEMAN, W. T. Pix3D: Dataset and Methods for Single-Image 3D Shape Modeling. In *2018 IEEE/CVF Conference on Computer Vision and Pattern Recognition* (Salt Lake City, UT, USA, June 2018), IEEE, pp. 2974–2983.
  - [32] TULSIANI, S., KAR, A., CARREIRA, J., AND MALIK, J. Learning Category-Specific Deformable 3D Models for Object Reconstruction. *IEEE Transactions on Pattern Analysis and Machine Intelligence* 39, 4 (Apr. 2017), 719–731.
  - [33] URBACH, D., BEN-SHABAT, Y., AND LINDENBAUM, M. Dpdist: Comparing point clouds using deep point cloud distance. In *European Conference on Computer Vision (2020)*, Springer, pp. 545–560.
  - [34] WAGNER, N., AND SCHWANECHE, U. NeuralQAAD: An Efficient Differentiable Framework for Compressing High Resolution Consistent Point Clouds Datasets. In *Proceedings of the 17th International Joint Conference on Computer Vision, Imaging and Computer Graphics Theory and Applications* (Online Streaming, — Select a Country —, 2022), SCITEPRESS - Science and Technology Publications, pp. 811–822.
  - [35] WANG, L., LI, X., AND FANG, Y. Deep-3daligner: Unsupervised 3d point set registration network with optimizable latent

- vector. *arXiv preprint arXiv:2010.00321* (2020).
- [36] WANG, M., WANG, L., AND FANG, Y. 3densinet: A robust neural network architecture towards 3d volumetric object prediction from 2d image. In *Proceedings of the 25th ACM international conference on Multimedia* (2017), pp. 961–969.
  - [37] WANG, N., ZHANG, Y., LI, Z., FU, Y., LIU, W., AND JIANG, Y.-G. Pixel2mesh: Generating 3d mesh models from single rgb images. In *Proceedings of the European conference on computer vision (ECCV)* (2018), pp. 52–67.
  - [38] WU, S., RUPPRECHT, C., AND VEDALDI, A. Unsupervised Learning of Probably Symmetric Deformable 3D Objects from Images in the Wild (Extended Abstract). In *Proceedings of the Thirtieth International Joint Conference on Artificial Intelligence* (Montreal, Canada, Aug. 2021), International Joint Conferences on Artificial Intelligence Organization, pp. 4854–4858.
  - [39] WU, T., PAN, L., ZHANG, J., WANG, T., LIU, Z., AND LIN, D. Density-aware chamfer distance as a comprehensive metric for point cloud completion. *arXiv preprint arXiv:2111.12702* (2021).
  - [40] XIE, H., YAO, H., SUN, X., ZHOU, S., AND ZHANG, S. Pix2Vox: Context-Aware 3D Reconstruction From Single and Multi-View Images. In *2019 IEEE/CVF International Conference on Computer Vision (ICCV)* (Seoul, Korea (South), Oct. 2019), IEEE, pp. 2690–2698.
  - [41] YI-SHENG, Z., GUO-FU, D., YONG, H., AND XU, M.-H. Fast intersection algorithm between spatial triangles [j]. *Application Research of Computers* 10 (2008), 2906–2910.
  - [42] YU, H., CHEANG, C., FU, Y., AND XUE, X. Multi-view Shape Generation for 3D Human-like Body. *ACM Transactions on Multimedia Computing, Communications, and Applications* (Feb. 2022), 3514248.